Stability Affects of Artificial Viscosity in Detonation Modeling

P. Vitello and P. Clark Souers, Energetic Materials Center
Lawrence Livermore National Laboratory
Livermore, CA, 94550

Accurate multi-dimensional modeling of detonation waves in solid HE materials is a difficult task. To treat applied problems which contain detonation waves one must consider reacting flow with a wide range of length-scales, non-linear equations of state (EOS), and material interfaces at which the detonation wave interacts with other materials. To be useful numerical models of detonation waves must be accurate, stable, and insensitive to details of the modeling such as the mesh spacing, and the mesh aspect ratio for multi-dimensional simulations. Studies we have performed show that numerical simulations of detonation waves can be very sensitive to the form of the artificial viscosity term used. The artificial viscosity term is included in our ALE hydrocode to treat shock discontinuities. We show that a monotonic, second order artificial viscosity model derived from an approximate Riemann solver scheme can strongly damp unphysical oscillations in the detonation wave reaction zone, improving the detonation wave boundary wall interaction. These issues are demonstrated in 2D model simulations presented of the "Bigplate" test. Results using LX-17 explosives are compared with numerical simulation results to demonstrate the affects of the artificial viscosity model.

INTRODUCTION

Accurate numerical modeling of high explosive detonation is an important part of the Accelerated Strategic Computer Initiative (ASCI) at Lawrence Livermore National Laboratory (LLNL). A goal of this initiative is the replacement of highly empirical models with physically accurate numerical calculations. To treat applied problems that contain detonation waves one must consider reacting flow with a wide range of length-scales, with non-linear equations of state (EOS), and with material interfaces at which the detonation wave interacts with other materials. Two and three-dimensional hydrodynamic propagation of detonation waves over long periods of time and around complex shapes is a challenging proposition even for current massively parallel supercomputer systems. To be useful numerical models of detonation waves must be accurate, stable, and insensitive to details of the modeling such as the mesh spacing, and the mesh aspect ratio. Improvements to current numerical models must be made to satisfy these requirements. Studies we have performed show that numerical simulations of detonation waves can be very sensitive to the form of the artificial viscosity term used. We show that a monotonic, second order artificial viscosity model derived from an approximate Riemann solver scheme can strongly damp unphysical oscillations in the detonation wave reaction zone, improving the detonation wave boundary wall interaction.

COMPUTATIONAL APPROACH

There are many Reactive Flow code models that are often used for detonation initiation studies and less often for prompt detonation.[1-9] We have used in this study the JWL++ Reactive Flow model.[7-9] This model provides for simulation of prompt detonation with a minimum number of coefficients, and produces good results when comparing with the limited amount of experimental data.

In its simplest form, the JWL++ model has four parts. The first is the use of the Murnahan EOS to describe the unreacted explosive EOS

$$P_U = \frac{1}{n\kappa}\left(\frac{1}{v^n} - 1\right), \qquad (1)$$

where P_U is the pressure for the unreacted material and $v = \rho_o/\rho$ is the relative volume. The initial and current densities are respectively ρ_o and ρ. The second part is the use of a JWL EOS in the C-term form to describe the fully reacted explosive

$$P_R = Ae^{-R_1 v} + Be^{-R_2 v} + Cv^{-(1+\omega)} . \qquad (2)$$

This JWL may be calculated directly from the equilibrium thermochemical code CHEETAH with a slight adjustment to the detonation velocity. It needs no corrections for non-ideality.

The third and fourth parts of the model are the analytic pressure mixer

$$P = (1 - F^m)P_U + F^m P_R \quad , \qquad (3)$$

and the rate equation describing the transformation of the unreacted to the reacted explosive,

$$\frac{dF}{dt} = G(P + Q)^b (1 - F) \ . \qquad (4)$$

F is the reacted mass fraction and Q is the "so called" artificial viscosity. The pressure P takes the value of P_U when the material is unreacted, P_R when the material is fully reacted, and an intermediate value then the material is partially reacted. As is discussed in the following, in a numerical simulation, $P + Q$, gives the effective pressure which takes into account the affect of a local velocity gradient.

JWL++ can reproduce the Size Effect and detonation front curvature. It shows all the prompt detonation features displayed by the more complex Reactive Flow model Ignition & Growth.[6] Detailed comparisons of the analytic pressure mixer, equation (3), with more complex partially burned pressure models show that the detonation results are insensitive to the choice of pressure mixing model.[9] The calculations shown here were undertaken using JWL++ implemented in a 2-D Arbitrary-Lagrangian-Eulerian (ALE) hydrocode, which starts Lagrangian and relaxes the mesh as needed with time.

APPROXIMATE RIEMANN SOLVER

Detonation waves have highly non-linear structures. The stability of the shock wave and of the pressure profile in the reaction zone are sensitive to how the hydrodynamic equations are solved. The aspect that we address here is the form for the Q term, which can be based on an approximate Riemann solver scheme.

The Euler equations of gas dynamics in Lagrangian coordinates can be written in differential conservation-law form as

$$\frac{\partial U}{\partial t} + \vec{\nabla} \cdot \vec{F} = 0$$
$$U = \begin{bmatrix} 1/\rho \\ v \\ E \end{bmatrix}, \quad F = \begin{bmatrix} -v \\ P \\ vP \end{bmatrix} . \qquad (5)$$

A discrete representation of a solution for U in one-dimension can be given as

$$U_i^{n+1} = U_i^n - \frac{\delta t}{\delta m}(\tilde{F}_{i+1/2} - \tilde{F}_{i-1/2}) . \qquad (6)$$

In equation (6), i corresponds to a spatial cell center position (see Figure 1), $i+1/2$ corresponds to cell boundary position, and n gives the time level. U_i^n and U_i^{n+1} correspond to the spatial cell averaged values of the physical variables at the beginning and end of the timestep. Note that for Lagrangian coordinates $\delta m = \rho \delta x$ corresponds to a mass increment.

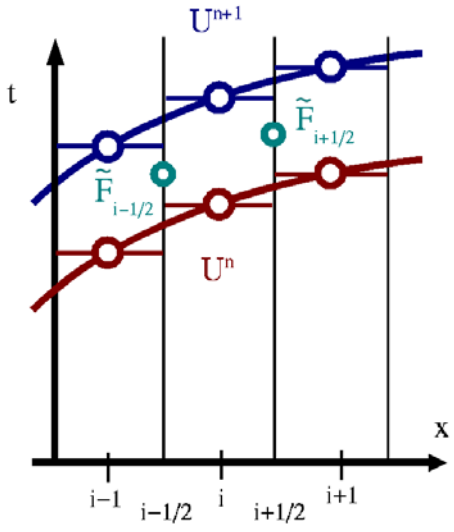

FIGURE 1. DISCRETE SOLUTION OF U.

The discrete solution of equation (6) can be viewed as a series of localized Riemann problems followed over a time period δt. The

Riemann problem is the initial value problem in the domain $-\infty < x < \infty$, $t > 0$ with initial data $U(x,0) = \{U_L,\ x < 0;\ U_R,\ x > 0\}$. For the gas dynamic equations, the Riemann solution always has discontinuities and consists of three waves, as is shown in Figure 2. The left and right waves are non-linear and may be either shock waves or rarefaction waves. The middle wave is always a contact discontinuity. Each wave carries information in an upwind manner and hence the resulting state will only depend on the local physical properties. In order to define completely the interaction between adjacent spatial cells, δt should be limited by the condition that adjacent Riemann problems do not interfere.

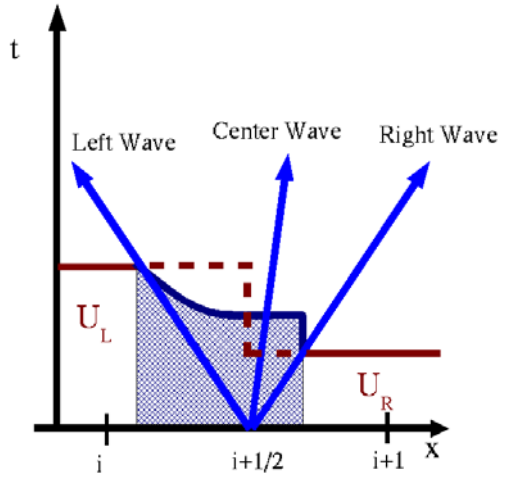

FIGURE 2. RIEMANN SOLUTION.

As was first demonstrated by Godunov[10], one can use the exact localized non-linear Riemann solution to calculate $\tilde{F}_{i+1/2}$. Godunov developed a three-step scheme to solve the discrete gas dynamic equations. The first step is to define a piecewise, cell averaged, representation of U at time level n (see Figure 1). Step two, which results in $\tilde{F}_{i+1/2}$, is to obtain the local Riemann problem at cell interfaces. The final step is to average the variables spatially after a time interval δt to provide new starting values for U.

Solving the non-linear Riemann problem for real gases is not practical for large multi-dimensional calculations. Approximate Riemann solvers replace the non-linear wave structure of the exact solution with a reduced number of linear waves. The use of linear waves makes non-iterative solutions possible. Since the discrete numerical schemes used in the numerical model already assume spatial averaging, an approximate solution to the Riemann problem can do nearly as good a job as an exact solution.

Using an upwind spatial differencing scheme, the flux can be approximated as

$$\begin{aligned}\tilde{F}_{i+1/2} &\approx \frac{1}{2}\left[F(U_{i+1}) + F(U_i)\right] \\ &\quad - \frac{1}{2}\left|\delta\tilde{F}_{i+1/2}\right| \\ &\approx \frac{1}{2}\left[F(U_{i+1}) + F(U_i)\right] \\ &\quad - \frac{1}{2}\left|\tilde{A}(U_{i+1}, U_i)\right|(U_{i+1} - U_i)\end{aligned} \quad , \qquad (7)$$

where in the limit that $U_i = U_{i+1}$, $\tilde{A}$ is the Jacobian of $\tilde{F}$ with respect to U. How one approximates the Riemann problem determines the value of $\tilde{A}$. The scheme in equation (7) is first-order in space as shown. This is due to the use of piecewise constant values for the cell center U_i values which results in the assumption that U_L and U_R for the Riemann problem discontinuity at $i+1/2$ are equal respectively to U_i and U_{i+1}. With a replacement of U_i and U_{i+1} by their extrapolated values, as in the MUSCL method, second order or higher spatial accuracy can be achieved.[11] The correction term $-\frac{1}{2}\left|\delta\tilde{F}\right|$ in equation (7) can be expanded in terms of a sum over characteristic waves variables w, leading to

$$\begin{aligned}\tilde{F}_{i+1/2} &\approx \frac{1}{2}\left[F(U_{i+1}) + F(U_i)\right] \\ &\quad - \frac{1}{2}\tilde{\rho}\sum_j \left|\tilde{\lambda}^j_{i+1/2}\right|\left(w^j_{i+1} - w^j_i\right)\tilde{r}^{\,j}\end{aligned} \quad . \qquad (8)$$

For an ideal gas with adiabatic index γ, the eigenvalues, $\tilde{\lambda}$, and eigenvectors, $\tilde{r}$, of $\tilde{A}$ are

$$\tilde{\lambda} = \begin{bmatrix} 0 \\ \tilde{c} \\ -\tilde{c} \end{bmatrix} \quad , \qquad (9)$$

and

$$\tilde{r} = \begin{bmatrix} -\frac{1}{\tilde{\rho}^2} & -\frac{1}{2\tilde{\rho}\tilde{c}} & \frac{1}{2\tilde{\rho}\tilde{c}} \\ 0 & \frac{1}{2} & -\frac{1}{2} \\ -\frac{\tilde{\rho}^2}{\gamma(\gamma-1)} & \frac{\tilde{u}\tilde{c}+\frac{\tilde{c}^2}{\gamma}}{2\tilde{c}} & \frac{\tilde{u}\tilde{c}-\frac{\tilde{c}^2}{\gamma}}{2\tilde{c}} \end{bmatrix} \quad (10)$$

with $\tilde{c}$ being the effective sound speed. The variables $\tilde{\rho}$, $\tilde{u}$, and $\tilde{c}$ are functions of U_i and U_{i+1}, and their value again depends on how one approximates the Riemann problem. The differences in the characteristic variables are

$$\delta w = \begin{bmatrix} \delta\rho - \frac{\delta P}{\tilde{c}^2} \\ \delta u + \frac{\delta P}{\tilde{\rho}\tilde{c}} \\ \delta u - \frac{\delta P}{\tilde{\rho}\tilde{c}} \end{bmatrix} . \quad (11)$$

In many implementations of a Lagrangian or ALE hydrocode, including the one used in this study, the material density and energy are calculated at cell centers, and the velocity is calculated at cell boundaries. For this staggered mesh spatial differencing scheme there are two Riemann problems. The velocity Riemann problem occurs at the cell center, with conditions of $\delta P = 0$, $\delta\rho = 0$, and finite δv. The density and energy Riemann problem occurs at cell boundaries with finite δP and $\delta\rho$, and $\delta v = 0$.

For the velocity Riemann problem $\left|\delta\tilde{F}\right|$, is given by

$$\left|\delta\tilde{F}\right| = \begin{bmatrix} 0 \\ \tilde{\rho}\tilde{c}\,\delta v \\ \tilde{\rho}\tilde{c}\tilde{v}\,\delta v \end{bmatrix} . \quad (12)$$

Using the second component of equation (12) results in the discrete velocity equation

$$v_{i+1/2}^{n+1} = v_{i+1/2}^{n} - \frac{\delta t}{\rho_{i+1/2}\delta x}(\tilde{P}_{i+1} - \tilde{P}_i) , \quad (13)$$

with the effective pressure being $\tilde{P} = P - \frac{1}{2}\tilde{\rho}\tilde{c}\,\delta v = P + Q$, with Q defined as

$$Q = -\frac{1}{2}\tilde{\rho}\tilde{c}\,\delta v . \quad (14)$$

The third component of equation (12) represents the correction to the energy equation resulting from a replacement in equation (5) of P with $P + Q$. For staggered mesh variables, it is sufficient to consider only the velocity equation Riemann problem and the resulting corrections to the Euler equations. Note that like P, Q is a cell-centered quantity.

We now need to proscribe how to calculate $\tilde{\rho}$ and $\tilde{c}$. To do so we make use of the Harten-Lax-van Leer[12] (HLL) approximate Riemann solver, which is one of the simplest schemes. It uses two waves separating a single constant intermediate state. The wave speeds are left as parameters to be determined. For the HLL model, Christensen[13] proposed the use of equal magnitude wave speeds of the form

$$\tilde{c} = c_o + \alpha\left|\delta v\right| . \quad (15)$$

based upon an empirical relation from particle-velocity/shock-velocity plots. In equation (15), c_o is the sound speed in the unshocked material and α is a material dependent quantity depending on the EOS. The α parameter can be given in terms of the ratio of the shocked to initial density as

$$\alpha = \frac{\frac{\rho_S}{\rho_o}}{\frac{\rho_S}{\rho_o} - 1} , \quad (16)$$

in the limit of very strong shocks.[14] The density $\tilde{\rho}$ to be used in calculating Q should be the local unshocked density. The resulting form for Q is

$$Q_i = \frac{1}{2}\rho_i\left(c_i + \alpha\left|\delta v\right|\right)\delta v . \quad (17)$$

To improve the accuracy of the differencing scheme the variable extrapolation the method (MUSCL) is used when evaluating δv in Q. In this method we replace the piecewise constant approximation of U_i with a piecewise linear approximation. The slopes of the linear variations have to be limited in order to avoid

overshoots in the numerical solution. Overshoots are avoided if the interface values remain between the adjacent average cell values. In order to ensure this monotonically condition, limiters are used in the definition of the interface value. For a uniformly spaced mesh, variable extrapolation gives

$$\delta v = v^R - v^L , \tag{18}$$

with

$$\begin{aligned} v^R &= v_{i+1/2} - \frac{1}{2}\Phi^R\left(v_{i-1/2}, v_{i+1/2}, v_{i+3/2}\right) \\ &\quad \times \left(v_{i+3/2} - v_{i+1/2}\right) \\ v^L &= v_{i-1/2} + \frac{1}{2}\Phi^L\left(v_{i-3/2}, v_{i-1/2}, v_{i+1/2}\right) \\ &\quad \times \left(v_{i-1/2} - v_{i-3/2}\right) \end{aligned} . \tag{19}$$

The limiters Φ given by Christensen[13] were used. For regions of locally smooth variation, Φ = 1, and δv will be approximately zero to third order, leading to the affect of Q being negligible away from sharp discontinuities.

For the velocity equation, Q represents a damping correction to the acceleration. In the energy equation, Q gives an effective viscous heating. Both positive and negative Q contribute to the heating. This is evident if one considers the Q contribution to the $-\widetilde{P}dV$ work. In one dimension, the $\widetilde{Q}dV$ work is always positive since Q is positive during compression (negative dV), and negative during expansion (positive dV). Many Lagrangian and ALE schemes restrict Q to be positive only. This limits the stabilizing affects of Q's pressure correction to regions of compression, but not expansion. There is no physical reason to limit Q. The sign of δv played no role in our Riemann problem based derivation of Q.

For standard, non-reacting shock waves the positive only restriction to Q can be beneficial as it can reduce numerical heating in regions of adiabatic expansion. Proper variable extrapolation has the same effect. For detonation waves, restricting Q to apply to only compression regions only can lead to unphysical oscillations in the reaction zone behind the shock front where there is a rapid decrease in pressure and density.

Results will be presented here for both positive only and unrestricted Q. While representing only a small fraction of the total effective pressure, we show that the wave damping contribution of Q can strongly contribute to numerical accuracy.

The BIGPLATE EXPERIMENT

We have used the "Bigplate" experiment[15] to demonstrate the affect of the Q pressure correction term. Bigplate is a unique explosive test in that variable angles of incidence exist between the explosive and the metal being pushed. Figure 3 gives a schematic for Bigplate. A disk of explosive is pressed with a radius of 100 mm. The explosives are LX-14 (95.5% HMX, 4.5% estane) and TATB. The disk thickness is 40 mm for LX-17. A 0.5 mm oxygen-free copper plate is glued to one side of the explosive, and a point detonator is placed on the axis at the back. A hole is machined so the detonator is flush with the back. There is no support plate on the back. An ultrafine TATB hemisphere booster of 19 mm radius is used. The point detonator creates a spherical wave that hits the copper plate on the axis first, then each point later farther out on the radius.

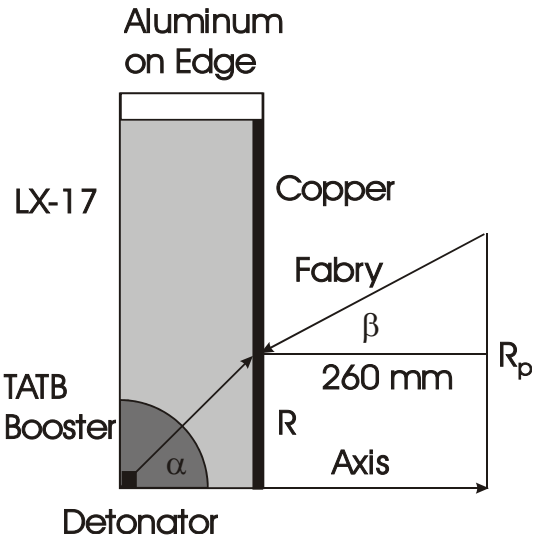

FIGURE 3. BIGPLATE GEOMETRY.

Five Fabry-Perot interferometer beams[16—17] are reflected off of the plate surface to measure the free-surface velocity. The beam diameters were about 1 mm. The initial radial positions, R, are: 0 (on the axis), 10, 20, 40 and 80 mm. The initial nominal Fabry angles, β, are 0, 4.5, 7.5, 10, and 11.5 degrees. These angles are selected to be about halfway between the initial and final plate positions. The radial distance defines the

geometric angle of incidence, α, which varies from 0° on the axis to 76° at 80 mm. The Fabry probes are set 260 mm from the front surface. Each probe was checked for he position of its light spot on the metal surface.

Each of the Fabry positions has two lengths. The fast Fabry starts before jump-off and runs about 2-3 μs. The slow Fabry starts about 1-2 μs before the end of the fast sweep and may run for 10 μs or more. Once the long Fabry is past its startup, it may be overlaid, with altering the times, with the short Fabry.

HYDRODYNAMIC CALCULATIONS

Numerical simulations were conducted using 0.125 mm axial spacing within the explosives, and 0.0417 mm axial spacing within the copper plate. The radial spacing is 0.125 mm within the explosives and the aluminum edge plate. Slide lines were placed between the explosive and metal. The TATB booster was modeled using programmed burn. For the booster region the lighting times were determined using experimental detonation velocity values. For LX-17, the detonation velocity is generated self-consistently using the JWL++ Reactive Flow model.

In Figures 4-5 we compare the calculated and experimental plate velocity at different radial points. The time axis for the simulated data was adjusted to agree with data for the axial Fabry curve. The dotted curves correspond to the experimental data. In Figure 4, *Q* was limited to be positive only, while both positive and negative values of *Q* were allowed in Figure 5. The experimental curves correspond to radial distances of 0, 1, 2, 4, and 8 cm from the axis. The calculated curves correspond to 0, 1, 2, 3, 4, 5, 6, 7, and 8 cm from the axis. We find very good agreement in both the timing of the jump-off of the plate and the final plate velocity. Values of the initial jump-off velocity are however very sensitive to how *Q* is treated. This is clearly evident in the curves at 2, 3, and 4 cm. With positive only *Q* (Figure 4), the jump-off velocity overshoots, and is then followed by a period of constant velocity. The experimental jump-off velocities decrease as we move outward from the axis. This behavior is reproduced using the *Q* model with both positive and negative values (Figure 5).

The calculated velocity curves for both *Q* models are compared in Figure 6. What is evident is that in addition to the velocity difference shortly after jump-off, there are long-term differences as well. Curves at 4 and 5 cm for the positive only *Q* model show lower velocities several μs after jump-off. This places the positive *Q* model calculated velocities for these curves under the experimental values.

Where *Q* is negative, it is never greater in magnitude than a few percent of the total pressure. Details in Figures 7-8 of the detonation wave pressure profiles near the copper plate show that even a small amount of negative *Q* pressure correction can lead to significant changes in the overall pressure profile. It is evident from Figures 7-8 that allowing *Q* to be negative results in a much smoother pressure profile. With only positive *Q*, the pressure profiles show strong oscillatory behavior. There is a evidence in Figure 7 for local minimums behind both the initial and reflected the shock peaks.

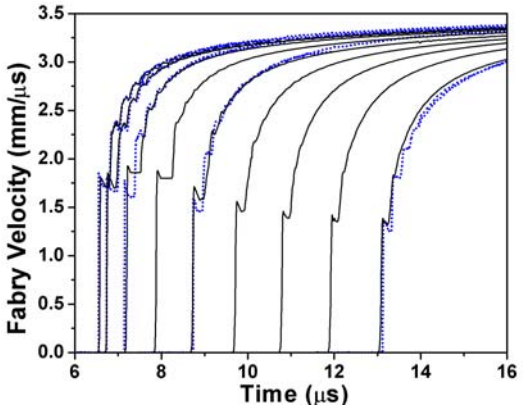

FIGURE 4. SOLID LINE: CALCULATED VELOCITY WITH Q LIMITED TO BE POSITIVE. DOTTED LINE: EXPERIMENTAL DATA.

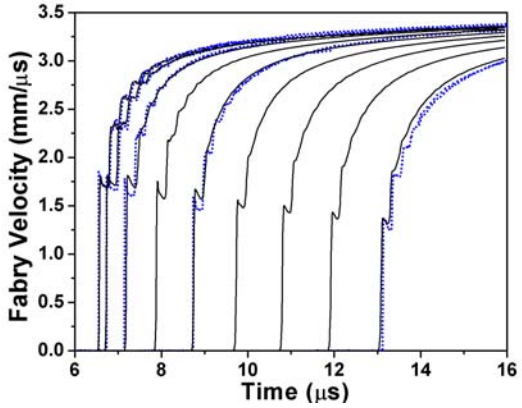

FIGURE 5. SOLID LINE: CALCULATED VELOCITY WITH Q POSITIVE AND NEGATIVE. DOTTED LINE: EXPERIMENTAL DATA.

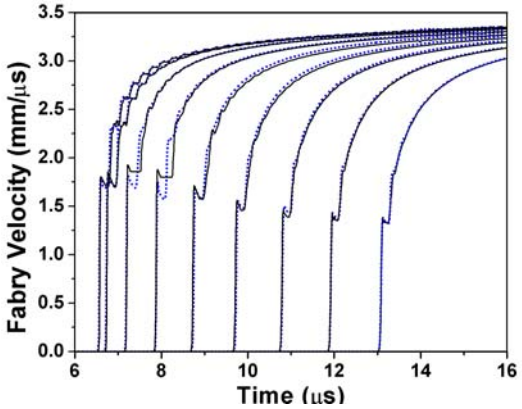

FIGURE 6. SOLID LINE: CALCULATED VELOCITY WITH Q LIMITED TO BE POSITIVE. DOTTED LINE: CALCULATED VELOCITY WITH Q POSITIVE AND NEGATIVE.

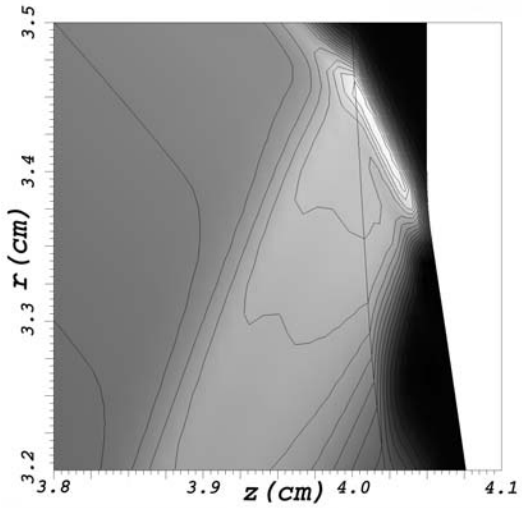

FIGURE 7. CALCULATED PRESSURE AT T=7 μs, WITH Q LIMITED TO BE POSITIVE WITH EQUALLY SPACED CONTOURS.

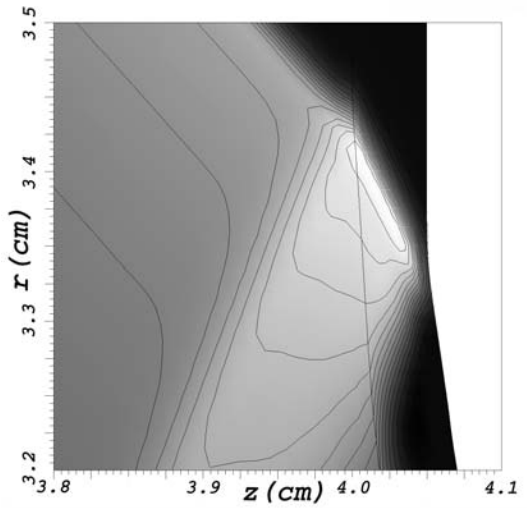

FIGURE 8. CALCULATED PRESSURE AT T=7 μs, WITH Q POSITIVE AND NEGATIVE WITH EQUALLY SPACED CONTOURS.

CONCLUSION

Many issues remain to be addressed before accurate, self-consistent multi-dimensional modeling of detonation waves in solid HE materials becomes a practical tool. The issue we have addressed here is the form for Q. We have shown that Q can be viewed as a pressure correction term derived from an approximate Riemann solver. Allowing Q to damp both compression and expansion oscillation is shown to result in smoother pressure profiles, which results in improved agreement with experimental data.

ACKNOWLEDGEMENTS

This work was performed under the auspices of the U. S. Department of Energy by the Lawrence Livermore National Laboratory under contract number W-7405-ENG-48.

REFERENCES

1. Leiper, G.A. and Cooper, J. "Reaction Rates and the Charge Diameter Effect in Heterogeneous Explosives," [Proc.] 9th (International) Symposium on Detonation, Portland, OR, August 28-September 1, 1989, pp. 197-206.

2. Tang, P. "Transition State Theory Applied to the Study of Reaction Processes in Detonation," Los Alamos National Laboratory Report LA-11903-MS, 1990.

3. Kennedy, D.L. and Jones, D.A.. "Modelling Shock Initiation and Detonation in the Non-Ideal Explosive PBXW-115," [Proc.] 10th (International) Symposium on Detonation, Boston, MA, July12-16, 1993, pp.665-674.

4. Cochran, G. and Chan, J. "Shock Initiation and Detonation in One and Two Dimensions," Lawrence Livermore National Laboratory Report UCID-18024, 1979.

5. Tarver, C.M., Tao, W.C., and Lee, C.G. "Sideways Plate Push Test for Detonation," Propellants, Explosives, Pyrotechnics, 21, 1996, pp. 238-246.

6. Lee, E.L. and Tarver, C.M. "Phenomenological Model of Shock Initiation in Heterogeneous Explosives," Phys. Fluids, 23, 1980, pp. 2362-2372.

7. Souers, P.C., Anderson, S., Mercer, J., McGuire, E., and Vitello, P. "JWL++: A Simple Reactive Flow Code Package for Detonation," Propellants, Explosives, Pyrotechnics, 25, 2000, pp. 54-58.

8. Souers, P.C., Anderson, S., McGuire, E., Murphy, M.J., and Vitello, P. "Reactive Flow and the Size Effect," Propellants, Explosives, Pyrotechnics, 26, 2001, pp. 26-32.

9. Souers, P.C., Garza, R., and Vitello, P. "Ignition & Growth and JWL++ Detonation Models in Coarse Zones," submitted to Propellants, Explosives, Pyrotechnics, 2002.

10. Godunov, S.K. "A difference scheme for numerical computation of discontinuous solution of hydrodynamic equations," Math. Sbornik, 47, 1959, pp. 271-306 (in Russian). Translated US Joint Publ. Res. Service, JPRS 7226, 1969.

11. Hirsch, C. "Numerical Computation of Internal and External Flows," Volume 2, John Wiley & Sons, 1991.

12. Harten, A., Lax, P.D., and van Leer, B. "On Upstream Differencing and Godunov-Type Schemes for Hyperbolic Conservation Laws," SIAM Review, 25, 1983, pp. 35-61.

13. Christensen, R.B. "Godunov Methods on a Staggered Mesh – An Improved Artificial Viscosity," Lawrence Livermore National Laboratory Report UCRL-JC-105269, 1990.

14. Dukowicz, J.K "A General, Non-Iterative Riemann Solver for Godunov's Method," J. Comp. Physics, 61, 1985, pp119-137.

15. Souers, P.C., Anderson, S., Avara, R., Fried, L., Janzen, J., McGuire, S., Wu, B. "Bigplate: An Oblique Angle Explosive EOS Test," Lawrence Livermore National Laboratory, UCRL-ID-131282, 1998.

16. McMillan, C.F., et al., "Velocimetry of fast surfaces using Fabry-Perot Interferometry," Rev. Sci. Instrum., 59, 1988, pp. 1-20.

17. Goosman, D.R., et al., "A dual, parallel cavity using Fabry-Perot Interferometry," Lawrence Livermore National Laboratory, UCRL-JC-116856, 1994.